



HAL
open science

Hydrogen diffusion and trapping in a low copper 7xxx aluminium alloy investigated by Scanning Kelvin Probe Force Microscopy

Loïc Oger, Manon Chloé Lafouresse, Grégory Odemer, Lionel Peguet,
Christine Blanc

► **To cite this version:**

Loïc Oger, Manon Chloé Lafouresse, Grégory Odemer, Lionel Peguet, Christine Blanc. Hydrogen diffusion and trapping in a low copper 7xxx aluminium alloy investigated by Scanning Kelvin Probe Force Microscopy. *Materials Science and Engineering: A*, 2017, 706, pp.126-135. 10.1016/j.msea.2017.08.119 . hal-03222780

HAL Id: hal-03222780

<https://hal.science/hal-03222780>

Submitted on 10 May 2021

HAL is a multi-disciplinary open access archive for the deposit and dissemination of scientific research documents, whether they are published or not. The documents may come from teaching and research institutions in France or abroad, or from public or private research centers.

L'archive ouverte pluridisciplinaire **HAL**, est destinée au dépôt et à la diffusion de documents scientifiques de niveau recherche, publiés ou non, émanant des établissements d'enseignement et de recherche français ou étrangers, des laboratoires publics ou privés.



Open Archive TOULOUSE Archive Ouverte (OATAO)

OATAO is an open access repository that collects the work of Toulouse researchers and makes it freely available over the web where possible.

This is an author-deposited version published in : <http://oatao.univ-toulouse.fr/>
Eprints ID : 19371

To link to this article : DOI:10.1016/j.msea.2017.08.119
URL : <http://dx.doi.org/10.1016/j.msea.2017.08.119>

To cite this version : Oger, Loïc and Lafouresse, Manon Chloé and Odemer, Grégory and Peguet, Lionel and Blanc, Christine *Hydrogen diffusion and trapping in a low copper 7xxx aluminium alloy investigated by Scanning Kelvin Probe Force Microscopy* (2017) *Materials Science and Engineering: A*, vol. 706, pp. 126-135. ISSN 0921-5093

Any correspondence concerning this service should be sent to the repository administrator: staff-oatao@listes-diff.inp-toulouse.fr

Hydrogen diffusion and trapping in a low copper 7xxx aluminium alloy investigated by Scanning Kelvin Probe Force Microscopy

Loïc Oger^{a,b}, Manon Chloé Lafouresse^a, Grégory Odemer^a, Lionel Peguet^b, Christine Blanc^{a,*}

^a CIRIMAT, Université de Toulouse, CNRS, INPT, UPS, ENSIACET, 4 Allée Emile Monso, BP 44362, 31030 Toulouse Cedex 4, France

^b Constellium Technology Center, 725 rue Aristide Bergès, CS 10027, 38341 Voreppe cedex, France

ARTICLE INFO

Keywords:

Aluminium alloys
Precipitation hardening
Fracture mode
Hydrogen diffusion
Hydrogen embrittlement (HE)
Scanning Kelvin Probe Force Microscopy (SKPFM)

ABSTRACT

The susceptibility to hydrogen embrittlement (HE) of the 7046 aluminium alloy (AA 7046) was investigated. Samples of AA 7046 corresponding to different ageing temperature/time couples were hydrogenated by cathodic charging in a H₂SO₄ solution. Scanning Kelvin Probe Force Microscopy (SKPFM) combined with global hydrogen amount measurements allowed apparent hydrogen diffusion coefficients (D_{app}) to be measured: the decrease of the D_{app} values with the increase of the ageing duration was attributed to hydrogen trapping by hardening η' and η precipitates for the aged alloy. Additional SKPFM measurements were carried out on hydrogen charged samples after desorption at 25 °C and combined with SEM observations of the fracture surfaces after tensile tests. Results showed that hydrogen could be trapped at the grain boundaries leading to brittle intergranular fracture. However, hardening precipitates could act as efficient trapping sites and reduce hydrogen trapping at the grain boundaries. Conclusion is that the most critical microstructural parameters for HE of AA 7046 correspond to the grain boundaries while ageing could contribute to improve the resistance to HE of the alloy by a well-controlled precipitation.

1. Introduction

Over the last few decades, environmental matters have been brought to the forefront in industrial policies. Concretely, the European automotive industry is currently impacted by standards requiring drastic reduction of the carbon dioxide emissions and thus of the fuel consumption [1]. Although steel is the reference material used in this industry, aluminium alloys are increasingly considered and 5xxx and 6xxx series are currently used for their low density close to 2.7 g cm⁻³ compared to 7.8 g cm⁻³ for steel [2]. However, in order to reach higher strength levels, Al-Zn-Mg-(Cu) alloys – the 7xxx series – are also being considered. However, as a function of composition and processing conditions, these alloys can be sensitive to stress corrosion cracking, so it is important to understand the mechanisms underlying their sensitivity [3].

Generally, HE is invoked to explain the susceptibility of the 7xxx alloys to stress corrosion cracking (SCC) [4]. Hydrogen can penetrate the alloy due to the cathodic reaction at the near surface balancing the metal dissolution in a corrosive solution. Hydrogen diffusion/transport is influenced by the stress gradients generated by a mechanical loading or by the forming process and can lead to a loss of the mechanical properties [5–7]. This generally results in a decrease of the elongation

to fracture [8] in relation with brittle fractures such as intergranular and cleavage [9]. These specific fracture modes can be related to critical microstructural trapping sites identified in the literature as grain boundaries [10,11], hardening precipitates [12], vacancies or dislocations [13]. As a matter of fact, hydrogen can easily be trapped in the tensile hydrostatic stress fields and on the contrary, it also distorts the metal lattice resulting in a decrease of the cohesion stresses [14].

This study attempts to provide some clarifications:

1. Firstly, on the role of hardening precipitates on hydrogen trapping and diffusion in a low copper content aluminium alloy, i.e. an AA 7046.
2. Secondly, on the role of trapped and diffusible hydrogen on the loss of mechanical properties in such an alloy.

Four metallurgical states were studied, corresponding to ageing from 0 to 48 h at 150 °C in order to make the nature and density of the hardening precipitates different from one sample to another. Hydrogen was introduced inside the material by cathodic charging. It is well known that it is very difficult to study hydrogen diffusion and trapping due to the size and mobility of this element. Based on recent works, it was decided in this work to use Scanning Kelvin Probe Force

* Corresponding author.

E-mail address: christine.blanc@ensiacet.fr (C. Blanc).

Table 1
Composition specification for AA 7046.

Element	Al	Zn	Mg	Cu	Fe	Si	Zr	Mn	Cr	Ti
wt%	Bal.	6.6–7.6	1.0–1.6	< 0.25	< 0.4	< 0.2	0.1–0.18	< 0.3	< 0.2	< 0.06

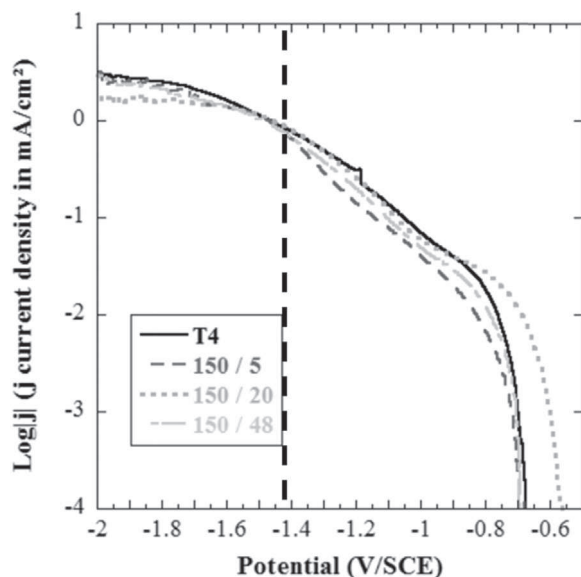


Fig. 1. Polarization curves for each metallurgical state of the AA 7046 in H_2SO_4 solution (pH 2) at 25 °C. Curves were plotted after 5 min of immersion at E_{corr} at a scanning rate of 250 mV h^{-1} .

Microscopy (SKPFM) to detect hydrogen [15–17]. Thus, hydrogen penetration depth was measured by SKPFM in the four states after cathodic charging. The resulting apparent diffusion coefficients (D_{app}) were evaluated in relation with the microstructural characteristics. These measurements were repeated after desorption at room temperature for several weeks. In addition, the fracture surfaces of pre-charged samples were observed after tensile tests and the depths of the brittle areas observed were related to the SKPFM measurements.

2. Experimental procedure

2.1. Specimen preparation

The AA 7046 of chemical composition given in Table 1 was investigated as 2 mm thick sheets in four different metallurgical states. 7xxx alloys without Cu are used in high volumes for automotive crash management systems. They have also excellent mechanical properties, weldability and cosmetic corrosion resistance for automotive applications. Due to its good corrosion resistance, AA 7046 allows the effect of H coming from chemical and electrochemical reactions to be evaluated without corrosion products disturbance. The reference metallurgical state, called T4, was hot rolled, cold rolled, solution heat treated and then stored at room temperature until substantially stable. The other metallurgical states were obtained from T4 plates by heat treatments at 150 °C for respectively, 5, 20 and 48 h. They were called as 150/5, 150/20 and 150/48 samples by reference to the ageing temperature/time couple. For all the experiments, the samples were cut from the sheets and were ground with abrasive paper SiC 1200 before being mechanically polished with diamond paste until 1 μm .

2.2. Analysis of the microstructure

The coarser precipitates were characterized by optical microscopy (OM Olympus PMG3) and by scanning electron microscopy (SEM

LEO435VP) coupled with Energy Dispersive X-ray Spectroscopy (EDS IMIX analyser) technique. SEM was also used to observe the fracture surfaces of the alloy after tensile tests.

Deeper investigations of the microstructure required the use of transmission electron microscopy (TEM JEOL-JEM-2010). For these observations, the samples were prepared as follows: ground with abrasive paper SiC 1200 until a thickness of 100 μm , mechanically cut in discs of 3 mm diameter and electropolished in a solution (CH_3OH : 900 mL, HNO_3 : 300 mL) at $-15 \text{ }^\circ\text{C}$ in a TenuPol-5. The precipitates were also characterized by using an EDX analyser with a spot size varying from 1.5 to 30 nm, by plotting their electronic diffraction patterns or by using high-resolution TEM (HRTEM).

2.3. Hydrogen charging

Specimens were cut from the AA 7046 sheets as parallelepipeds of $15 \times 4 \times 2 \text{ mm}^3$ with a mass of $(300 \pm 10) \text{ mg}$. Hydrogen was inserted by cathodic charging at $25 \pm 2 \text{ }^\circ\text{C}$ in a pH 2 H_2SO_4 solution: during the charging, only the longitudinal (L) – long transverse (LT) plane was exposed to the electrolyte, all other planes being protected by a transparent lacquer. A three-electrode system made of the specimen as working electrode, a Pt counter electrode and a saturated calomel electrode (SCE) as reference, all electrodes being connected to a Biologic potentiostat, was used to apply a potential of -1.450 V vs SCE for 72 h. This potential was chosen because, in the electrolyte chosen, the resulting current density is similar for the four metallurgical states (Fig. 1). This potential also corresponds to the transition between the oxygen and the hydrogen reductions which could explain the time duration required for the current density to stabilize during the charging. It allowed slowing down the alteration of the surface.

2.4. Hydrogen amount measurements

2.4.1. Global measurements: by melting method

A Bruker G8 GALILEO Instrumental Gas Analyser (IGA) was used to measure the global amount of hydrogen contained in the samples melted in graphite crucibles. The catharometric method based on the difference of thermal conductivity of the vector gas (Ar) with and without hydrogen allowed a sensitivity of 1 ppm for samples of approximately 300 mg. Moreover, this method requires no vacuum that could lead to hydrogen desorption. The dimensions of the coupons were similar to that of the charged tensile test samples and their near surface was slightly polished using a 1200 SiC paper before the measurement in order to limit the presence of hydrogen related to the formation of a thin oxide film [18]. Each measurement was repeated at least five times for reproducibility.

2.4.2. Local investigations by SKPFM

The hydrogen penetration depth was investigated using SKPFM on a 5500 Agilent Atomic Force Microscope (AFM). Both topography and surface potential signals were acquired simultaneously (single pass mode). The probes were conductive Pt-coated silicon tips. In the single pass mode set up, the tip is vibrated above the surface at two different frequencies: a frequency close to the resonant frequency of the tip (300 kHz) by mechanical excitation in order to control the tip-sample distance and a lower frequency (10 kHz) by electrical excitation to measure the surface potential [19]. Amplitude modulation (AM) - KFM mode was used in order to have the best spatial resolution possible (approximately 50 nm). In this mode, a voltage $V_{dc} + V_{ac} \sin(\omega t)$ is

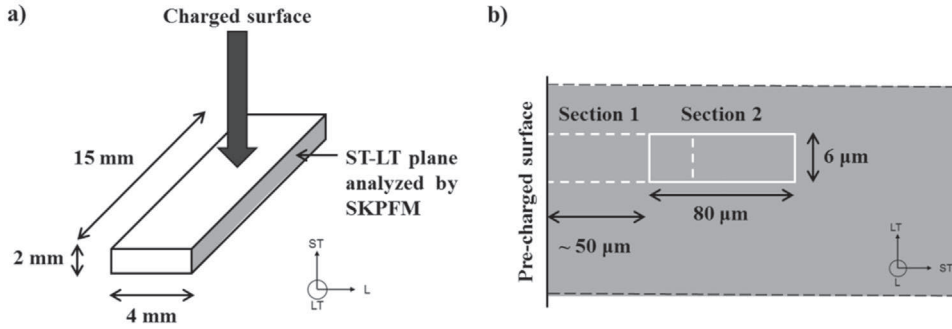


Fig. 2. a) Dimensions of the coupons analysed by SKPFM, b) Scheme of the data treatment method applied.

applied to the tip. The resulting oscillating potential difference between the tip and sample modulates the electrostatic force between the tip and the sample inducing an oscillation of the tip. V_{dc} is adjusted, until the amplitude of the oscillations is minimal, which occurs when V_{dc} is equal to the potential difference between the tip and the sample. This set up allows a high spatial resolution. Another advantage of this method is that measurements require no vacuum. All SKPFM measurements were performed in air at room temperature. For a given condition, the measurements were repeated at least three times for reproducibility.

After hydrogen charging, the coupons were cut and polished and the SKPFM measurements were conducted on cross-sections in the LT- short transverse (ST) plane (Fig. 2a and b). The time between charging and SKPFM measurements was estimated to be 20 min. The LT-ST plane was previously polished with $\frac{1}{4}$ μm diamond paste. Rectangular sections of $80 \mu\text{m} \times 6 \mu\text{m}$ were successively scanned from the charged surface up to $400 \mu\text{m}$ in the core of the sample in the ST direction. An increment of $50 \mu\text{m}$ was applied with a micrometer screw between each section in order to precisely evaluate the depth analysed by matching topography measurements. An overlap of the potential value of the two adjacent images ensured that the surface potential value was stable. Results were analysed with the *Gwyddion* software.

2.5. Mechanical properties

The mechanical properties of the alloy were studied on specimens machined in the LT direction. Samples with a parallelepiped gauge section of $23 \times 1.9 \times 2.8 \text{ mm}^3$ were used. Tensile tests were carried out at a strain rate of 10^{-3} s^{-1} at room temperature in a dual column MTS testing machine with a frame capacity of 30 kN. Healthy and pre-hydrogenated samples were tested in order to highlight the effects of the hydrogen on the mechanical properties. The time between charging and tensile testing was estimated to be 15 min. For brevity, we chose to present the results for only the AA 7046-T4 and 150/20 samples.

The ageing at 150°C modifies the volume fraction, size distribution and the nature of the hardening precipitates. This was controlled by hardness measurements on a *BUEHLER-Omnimet 2100* tester equipped with a Vickers indenter. A load of 500 g was chosen taking into account the samples thickness.

All mechanical tests were repeated at least three times for reproducibility allowing error bars to be added on the corresponding figures.

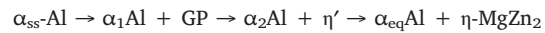
3. Results and discussion

3.1. Evolution of the AA 7046 microstructure with ageing

The AA 7046-T4 presented an equiaxed microstructure in good agreement with the manufacturing process applied. A precise study of the grain size in each plane of the sheets revealed no preferential orientation of the grains and no change of their size from one plane to another. At the OM and SEM scales, all the metallurgical states studied had a very similar microstructure. OM and SEM observations showed,

for all metallurgical states, coarse intermetallic particles smaller than $10 \mu\text{m}$ and identified by EDX as Al_3Fe and Al_3Ti . In-depth analyses by TEM confirmed these results and also revealed the presence of coherent spherical Al_3Zr dispersoids with an average diameter of $42 \pm 3 \text{ nm}$ that were formed during the homogenization [20]. The nature of these phases was confirmed by analysing their diffraction patterns [21]. Intergranular precipitates were also observed and characterized as MgZn_2 particles in all metallurgical states.

TEM observations also showed that the ageing affected the nature and size of the hardening precipitates, the size of the intergranular precipitates and the width of the precipitate free zone (PFZ) as shown in Fig. 3. The precipitation sequence in Al-Zn-Mg alloys was well investigated in several works [22–24] and can be described by the following sequences in alloys with a Zn/Mg ratio higher than 1 and with a low Cu amount:



where α_{ss} , α_1 , α_2 and α_{eq} represent the composition of the solid solution for each step of the precipitation sequence.

At first, during the natural ageing, Zn and Mg progressively co-segregated to form Guinier-Preston (GP) zones responsible for the precipitation of metastable η' -phases and finally stable η - MgZn_2 phases which occurs at higher temperature. In the T4 state (Fig. 3a), no GP zone was observed even using HRTEM and although their presence was highly suspected especially because of the long natural ageing duration and the high hardness value (Fig. 4a), the GP zones being known to favour the hardening of these alloys [24]. After 5 h of ageing, a slight change in the microstructure was noticeable, with thin intragranular precipitates that cannot be seen easily in Fig. 3b but were well observed and accurately identified using hardness measurements (Fig. 4a) and HRTEM observations combined with diffraction patterns (Fig. 4b). HRTEM images (Fig. 4b) showed semi-coherent precipitates in the 150/5 sample which are generally attributed to the η' -phase. Although the composition of these precipitates could not be precisely identified because of their size, EDX analyses performed in the area containing the precipitates showed a composition very close to that found in the work of Dumont et al. [25] for η' precipitates and different from the MgZn_2 precipitates identified in the grain boundaries. Moreover, the hardness increase (Fig. 4a) highlighted the hardening properties of these particles. Coupling all these characteristics with the literature review indicated that the particles observed were actually η' precipitates [24,26]. In comparison, the 150/20 and 150/48 samples showed more obvious microstructural changes visible respectively in Figs. 3c and 3d. A dense hardening precipitation was observed in the grains and coarsened from 20 to 48 h of ageing. Fig. 4c shows a micrograph of the intragranular precipitates observed in the 150/48 samples (same observation for the 150/20 samples). The higher size of the precipitates made analyses easier and HRTEM images coupled with EDX allowed these phases to be identified as stable η - MgZn_2 in both states. This was confirmed by the diffraction pattern given in Fig. 4d. Obviously, these states were assumed to contain both η' and η precipitates but with a dominant amount of the latter [25]. The decrease of the hardness observed in

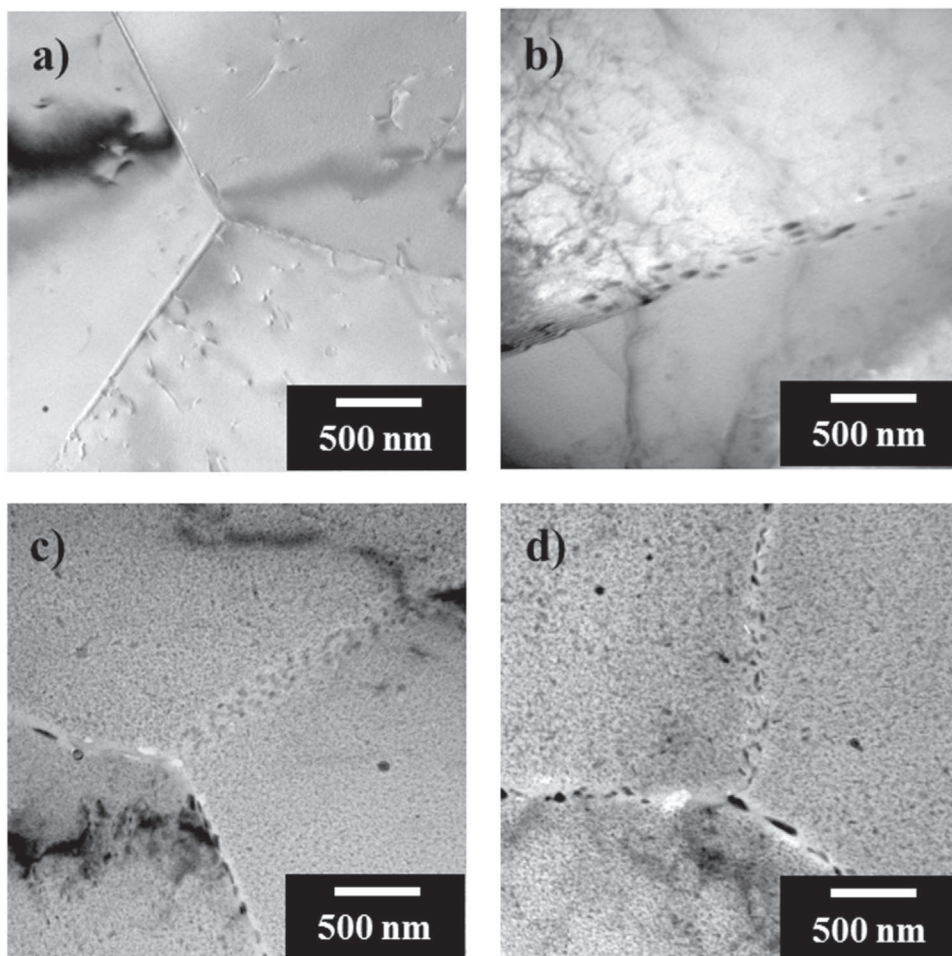


Fig. 3. TEM micrographs showing the microstructural change with the ageing duration: a) T4 state, reference b) sample aged for 5 h at 150 °C (150/5), c) sample aged for 20 h at 150 °C (150/20), d) sample aged for 48 h at 150 °C (150/48).

Fig. 4a was in good agreement with the results, due to the evolution of the η' -phase into the stable η -phase and the increase of the precipitate size [20] leading to a transition from a shearing mechanism to Orowan looping. The hardening is thus inversely proportional to the radius of the hardening precipitates [27,28]. Although the areas analysed during TEM observations were not fully representative of the global microstructure, an analysis of the particle size revealed a slight increase from approximately 6 nm to 10 nm and to 17 nm for respectively 5, 20 and 48 h of ageing at 150 °C. This observation was in good agreement with the hardness evolution. Moreover, TEM observations (Fig. 3) showed the growth of the intergranular precipitates from T4 to 150/48 samples, with only some small (15 ± 6 nm) intergranular precipitates for the T4 state (Fig. 3a) compared to numerous 61 ± 25 nm intergranular precipitates for the 150/48 sample (Fig. 3d). The coarsening of the intergranular precipitates led to the growth of the PFZ which was approximately 50 nm wide for the 150/5 sample compared to 120 nm for both 150/20 and 150/48 samples.

3.2. Hydrogen charging

All metallurgical states were hydrogenated following the same conditions for 72 h. Fig. 5 gives an overview of the global hydrogen amount measured by IGA as a function of the ageing duration (error bars are calculated on the basis of 5 measurements). It could be reminded that the coupons were slightly polished (less than 5 μm) before IGA analysis. As a consequence, the hydrogen located under the near surface could have been underestimated. Nevertheless, it was assumed that comparison between the different metallurgical states was relevant. A slow decrease of the amount of hydrogen introduced in the

alloy was noticed from the T4 to the 150/5 sample and from the 150/5 to the 150/20 sample. Then, the quantity of hydrogen absorbed remained stable and no significant difference in the hydrogen amount was observed between the 150/20 and the 150/48 samples.

The global analysis of the hydrogen amount inserted in a sample was interpreted in terms of capability of hydrogen to diffuse and to be trapped. It is commonly assumed that the nature, size and distribution of hardening precipitates are major parameters for hydrogen trapping [29,30]. The misorientation between the particles and the matrix can lead to a loss of coherence and the elastic distortion near the interface can promote hydrogen stabilization [31]. Moreover, in some alloys [32], the distortion can be offset by an accumulation of dislocations, also reported to be hydrogen trapping sites. Results showed that, during the first 5 h of ageing, the most significant microstructural changes occurred with the increase of the hardening precipitates density. Concerning these intragranular precipitates, their interfaces with the matrix were only partly coherent and could act as barrier for hydrogen diffusion so that the hardening precipitates could be considered as trapping sites. However, for T4 and 150/5 samples, the main hardening precipitates were GP zones and η' precipitates which were associated with a compression of the lattice [28,33] and, therefore, limited the quantity of hydrogen possibly trapped. Between 5 and 20 h of ageing, another significant microstructural change occurred: the precipitates coalesced and their coherence with the matrix decreased with the formation of the η -phase [34]. The total length of the matrix/precipitate interfaces was higher and the stress fields generated led to lattice distortion which could explain that more hydrogen was trapped. Finally, between 20 and 48 h of ageing, the change of the particles size did not seem to affect the hydrogen trapping. Therefore, two parameters could supposedly be

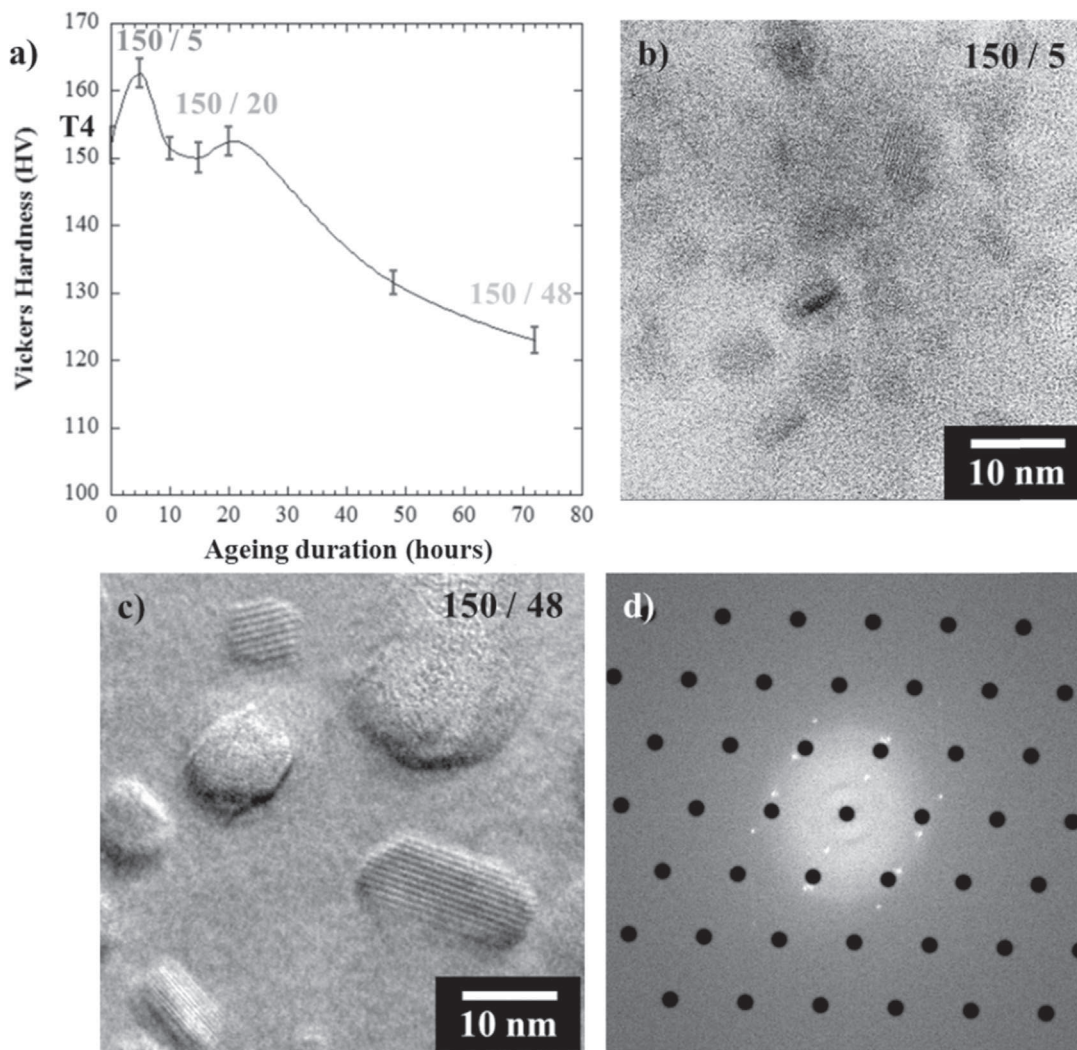


Fig. 4. a) Evolution of the Vickers Hardness (500 g load) with the ageing duration at 150 °C, b) HRTEM micrograph of hardening η' precipitates observed in the sample aged for 5 h at 150 °C (150/5), c) η -MgZn₂ precipitates observed with HRTEM in the sample aged for 48 h at 150 °C (150/48) and the corresponding diffraction pattern d) – superposition of the matrix diffraction oriented in [011] direction (•) and the η -MgZn₂ diffraction oriented in [215] direction (○).

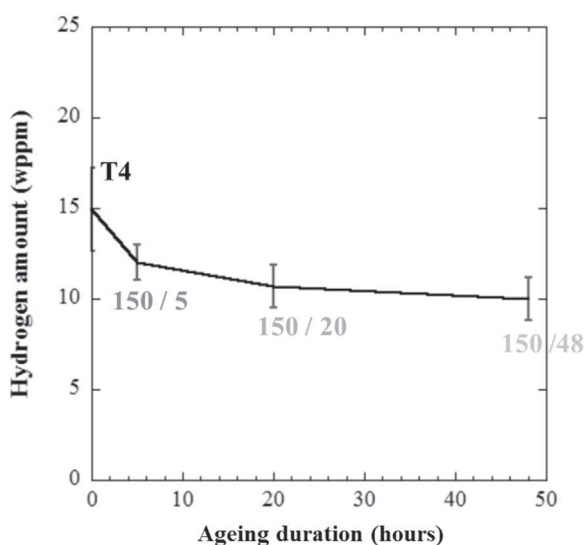


Fig. 5. Hydrogen amount measured with IGA after cathodic charging in H₂SO₄ pH 2 for 72 h as a function of the ageing duration.

considered to explain hydrogen trapping, i.e. the size of the particles and the coherence level of the matrix/precipitate interface [29]. Depending on these two parameters, a saturation level for hydrogen trapping could be defined for each type of precipitate.

3.3. Hydrogen diffusion investigation

In a first approach, hydrogen diffusion was investigated by using Secondary Ions Mass Spectroscopy (SIMS) but no evidence of the presence of hydrogen deeper than in the native oxide film was highlighted. This can be explained by the 10^{-8} mbar vacuum during SIMS analysis presumably low enough to make hydrogen desorb. Thus SKPFM measurements emerged as the best alternative to detect hydrogen in the material.

Fig. 6 shows a representative measurement of the surface potential (V) as a function of the depth from the near surface (i.e. the charging side for samples cathodically charged) for a non-charged AA 7046 T4 sample. For all measurements performed (five for these experiments), the surface potential remained stable except for local dips associated to the presence of intermetallic particles. In Fig. 6, an average value of the surface potential, close to 1.4 V, was measured but this value could change from a measurement to another due to small differences in temperature and relative humidity in the laboratory room. As a consequence, in the following, all measurements were normalized by

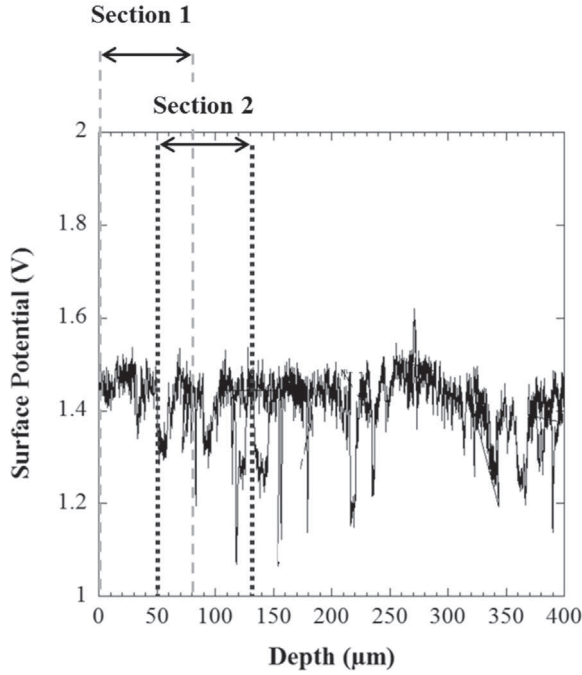


Fig. 6. Evolution of the surface potential (V) as a function of the depth for an uncharged AA 7046 T4 sample.

calculating ΔV which corresponded to the difference between the potential in the uncharged part of the sample, very far from the charging side, V_{∞} , and the measured potential at a distance x , V_x so that only the surface potential gradient was considered. Finally, it can be noticed that for a hydrogen-free sample, no potential gradient was observed; the same result was obtained for the four metallurgical states.

Fig. 7 shows the evolution of ΔV as a function of the depth from the hydrogen-charging side for each metallurgical state after 72 h of hydrogen charging in H_2SO_4 (pH 2). For all metallurgical states, a ΔV gradient was observed between the charged surface and the hydrogen-free core of the coupons. According to previous works, this gradient can be related to the presence of hydrogen that modifies the electronic output work [15]. Although no clear mechanism explaining the role of hydrogen on the electronic output work was established, it was assumed that hydrogen distorts the metallic lattice leading to the variations observed. It could be assumed that the response to hydrogen concentration should depend on the precipitation state. Indeed, the trapping sites distort the lattice and/or create interfaces at which the hydrogen atoms will distort the lattice less. However, regarding the diffusion distance, this was assumed not to affect the conclusions concerning the hydrogen diffusion distance even though it should affect the absolute Volta potential.

By this way, it was thus possible to determine the diffusion depth of hydrogen and then to calculate an apparent hydrogen diffusion coefficient, D_{app} . D_{app} values were evaluated by means of the analytical solution of Fick's second law:

$$\frac{c(x)-c_s}{c_0-c_s} = \text{erf}\left(\frac{x}{2\sqrt{D_{app}t}}\right) \quad (1)$$

In Eq. (1), $c(x)$ corresponds to the hydrogen concentration at a distance x from the surface exposed to the hydrogenating media, c_0 is the initial concentration in the bulk of the alloy ($c(x,0) = c_0 = 0$ for $t = 0$ and $x > 0$), c_s is the hydrogen concentration at the surface during the cathodic charging ($c(0,t) = c_s = 1$ for $t > 0$ and $x = 0$) and t is the charging time. SKPFM measurements did not allow diffusible and trapped hydrogen to be distinguished although, as previously discussed, several microstructural parameters are known as trapping sites. As a

consequence, the value of the hydrogen diffusion coefficient should be continuously modified taking into account the trapping during diffusion. In our case, the impossibility to implement the diffusion equation with this phenomenon led us to use an apparent hydrogen diffusion coefficient.

Comparison of the four graphs (Fig. 7) showed a decrease of the hydrogen diffusion depth corresponding to a decrease of D_{app} when the ageing duration increased. All measurements were summarized in Table 2.

The D_{app} values were smaller than those found in the literature for other materials, mainly for pure aluminium, and based on calculations and experimental measurements, closer to 10^{-8} – 10^{-9} $cm^2 s^{-1}$ [13,35]. This could be attributed to microstructural differences, especially to the GP zones and other thin precipitates that slowed down hydrogen diffusion for AA 7046. Nevertheless, the orders of magnitude remained close. The evolution of D_{app} was very similar to that of the hydrogen amount with a noticeable decrease from the T4 state down to the 150/20 sample and then a stabilization from the 150/20 to the 150/48 samples. This result was consistent with hardening precipitates acting as a barrier for hydrogen diffusion.

The absence of significant change in D_{app} between 20 and 48 h of ageing offered evidence for the coherence level of the precipitate/matrix interface as a major parameter concerning hydrogen trapping. Thus, η' precipitates would trap less hydrogen than η precipitates which, therefore, seemed to be more efficient to protect the alloy from HE. The volume fraction of the precipitates could also be considered to explain the result. However, a study of Dumont et al. [25] for a Cu-free 7xxx aluminium alloy showed no significant differences between a T6 and a T7 state in the precipitates volume fraction which should discredit this hypothesis. This question will be more precisely discussed in the following.

Finally, it could be also noted that the maximum value for the ΔV gradient, ΔV_{max} , between the surface and the core of the specimens varied between 200 and 400 mV depending on the metallurgical state (Fig. 7). The value of ΔV_{max} could be related to the hydrogen amount: the decrease of ΔV_{max} from T4 state to 150/20 state (Fig. 7) was then consistent with the decrease of the hydrogen amount when the ageing duration increased (Fig. 5). On the contrary, the increase of ΔV_{max} from the 150/20 to the 150/48 state was not explained at this time. But, previous comment concerning the influence of the microstructure on hydrogen ability to distort the lattice led us to assume that there is not a trivial relationship between hydrogen concentration and the Volta potential.

3.4. About the role of trapped hydrogen

Given the relationship 'microstructure – hydrogen diffusion and trapping' shown in the previous paragraph, it was of interest to evaluate the influence of hydrogen on the mechanical properties of AA 7046. In this part, the study was focused on two metallurgical states, corresponding to the T4 and 150/20 samples. Fig. 8 shows SEM micrographs of the fracture surfaces obtained for samples after hydrogen charging and tensile tests for both metallurgical states. For hydrogen charged samples, the observations were focused on the hydrogen affected zone. For comparison, fracture surfaces for hydrogen-free samples are also given. Figs. 8a and 8c showed that the fracture mode in the hydrogen-free T4 state is ductile intergranular in relation with intergranular precipitates [36]. For hydrogen-free 150/20 sample, the fracture mode was ductile transgranular with dimples (Figs. 8b and 8e). After hydrogen-cathodic charging, brittle intergranular fracture (Figs. 8d and 8g) and cleavage (Figs. 8d and 8h) areas were observed for the T4 metallurgical state. These fracture modes are known to be relevant evidences of HE. The brittle intergranular fracture mode clearly revealed the diffusion and trapping of hydrogen in the grain boundaries that led to a decrease of the intergranular cohesion stresses [37,38]. The co-existence of both brittle intergranular and cleavage areas could

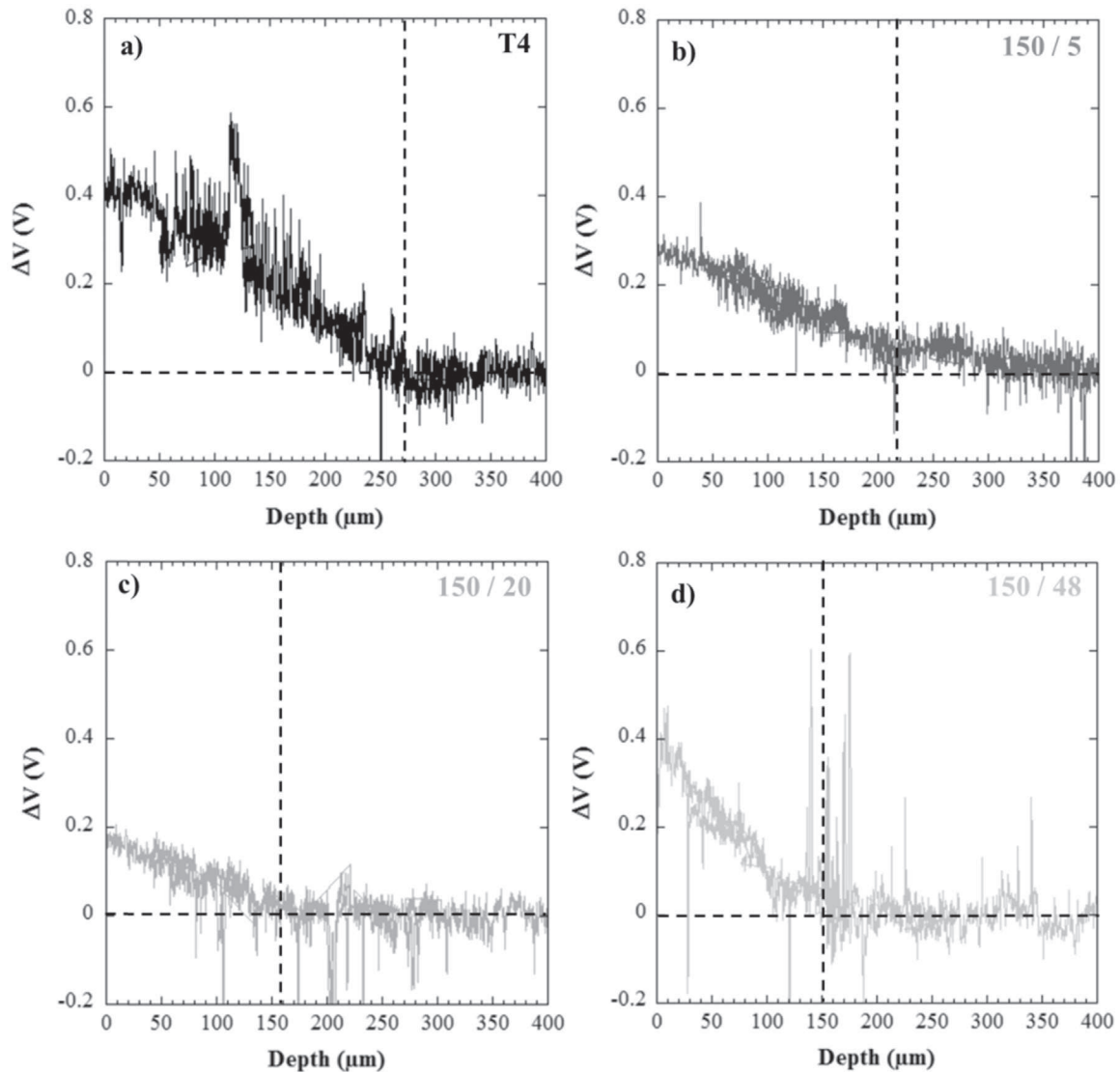


Fig. 7. Evolution of ΔV as a function of the depth from the hydrogen-charged surface after cathodic charging in H_2SO_4 (pH 2) for 72 h: a) T4, b) sample aged for 5 h at 150 °C (150/5), c) sample aged for 20 h at 150 °C (150/20), d) sample aged for 48 h at 150 °C (150/48).

Table 2

Evolution of the depth affected by hydrogen and apparent hydrogen diffusion coefficient for each metallurgical state.

State	T4	150/5	150/20	150/48
Depth (μm)	275 ± 15	230 ± 10	155 ± 10	150 ± 10
D_{app} ($cm^2 s^{-1}$)	$2-2.6 \times 10^{-10}$	$1.5-1.7 \times 10^{-10}$	$5.7-8 \times 10^{-11}$	$5-7 \times 10^{-11}$

be explained by local hydrogen concentrations: far from the charged surface, the hydrogen concentration in the grain boundaries was too low to induce intergranular fracture but the increase of the stress fields at the crack tip could explain the cleavage areas boarding the brittle intergranular areas. Further, the results led us to assume the decrease of the interplanar cohesion stress due to reticular hydrogen. For hydrogen-charged 150/20 samples, no change in the fracture mode was noticeable close to the charged surface compared to hydrogen-free samples (Fig. 8f). This result was consistent with previous conclusions about the role of the hardening precipitates and the evolution of the D_{app} coefficients. For 150/20 samples, η precipitates were assumed to trap the hydrogen and acted as a protection for the grain boundaries explaining why no intergranular fracture was observed. However, SKPFM

measurements showed that hydrogen penetrated inside the sample over more than 100 μm whereas no effect of hydrogen diffusion on fracture surfaces was visible.

For a better understanding, SKPFM measurements were carried out on hydrogenated samples after exposure for 3 weeks in ambient atmosphere. The results, displayed in Fig. 9, showed a drastic decrease of the depth altered by hydrogen in the T4 state, from approximately 270 μm (Fig. 7a) to about 75 μm (Fig. 9a) for samples tested immediately after hydrogen-charging and those tested after 3 weeks respectively. This could be related to the desorption of a large part of hydrogen during the exposure to ambient atmosphere. On the contrary, for the 150/20 sample, hydrogen was detected until an approximate depth of 160 μm (Fig. 9b) which was similar to the sample tested immediately after charging (Fig. 7c) and therefore, showed that no hydrogen had desorbed. This was consistent with hydrogen trapping at the hardening precipitates that could be considered as strong trapping sites [39]. SEM observations of the fracture surfaces for the T4 hydrogen-charged samples showed that the depth of the brittle intergranular fracture area was of approximately 70 μm (Fig. 8d), which corresponded to the depth where hydrogen was detected by SKPFM after 3 weeks of desorption (Fig. 9a). Comparison of the different results showed that SKPFM measurements did not allow the different

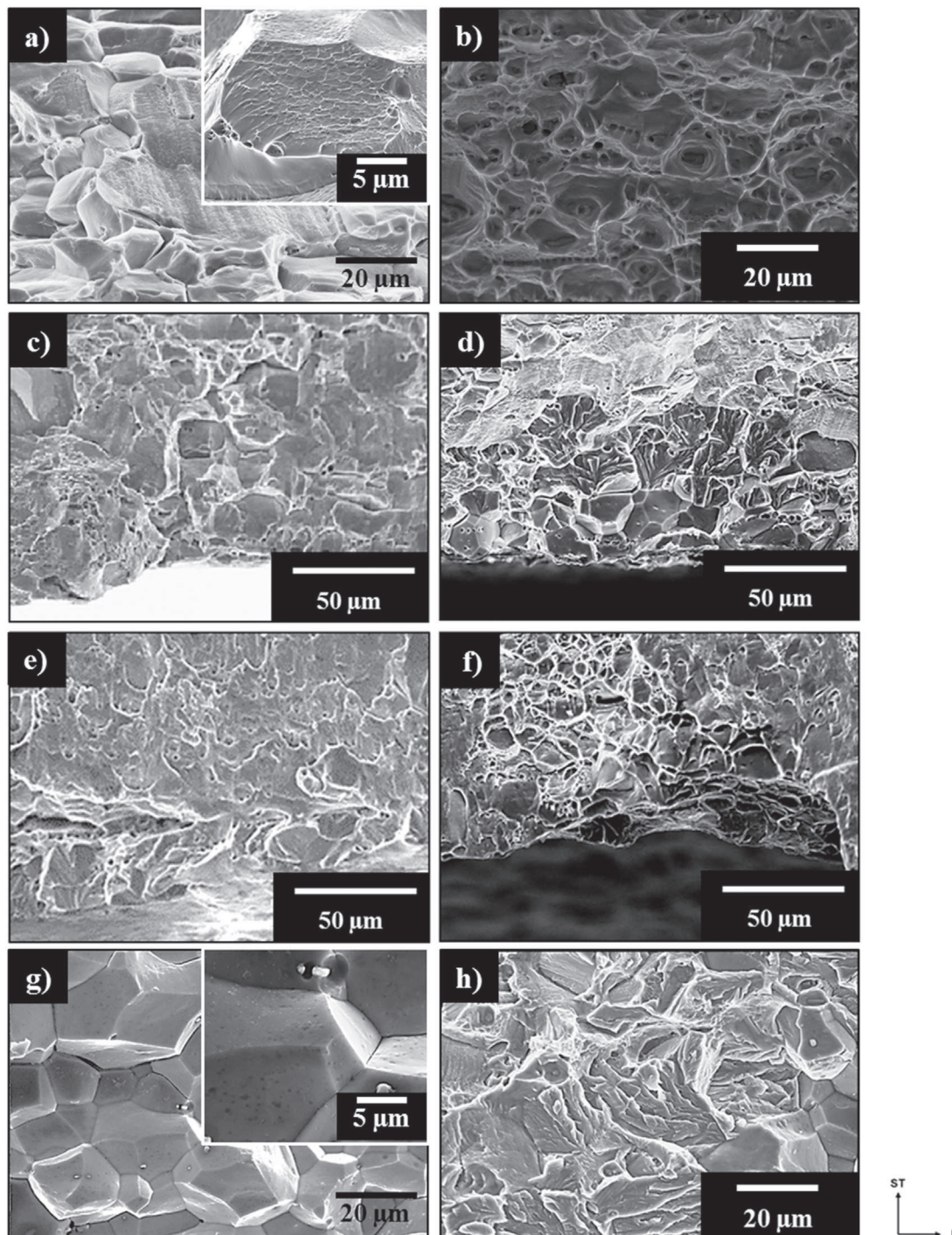


Fig. 8. SEM micrographs of the fracture surfaces obtained for AA 7046: a) ductile-intergranular fracture in the T4 state (bulk), b) ductile transgranular fracture for the samples aged for 20 h at 150 °C (150/20) (bulk), c) ductile-intergranular fracture in the T4 state (near the surface of the tensile sample), d) hydrogen-affected zone showing brittle intergranular and cleavage areas for T4 samples after charging for 72 h in H₂SO₄ (pH 2), e) ductile transgranular fracture for the samples aged for 20 h at 150 °C (150/20) (near the surface of the tensile sample), f) hydrogen-enriched zone for the samples aged for 20 h at 150 °C (150/20) after charging for 72 h in H₂SO₄ (pH 2), g) focus on d) showing brittle intergranular fracture, and h) focus on d) showing cleavage areas. Tensile tests were performed at 10^{-3} s^{-1} .

populations of hydrogen, i.e. diffusible and trapped hydrogen, to be distinguished. Further, the absence of hydrogen desorption for the 150/20 sample showed that the main part of the hydrogen inside the 150/20 sample corresponded to hydrogen trapped at the hardening precipitates which could not desorb at room temperature. Concerning the T4 samples, it was thus assumed that both diffusible and trapped hydrogen was present after charging while only diffusible hydrogen desorbed during the 3 weeks exposure at room temperature. According to the analysis of the T4 microstructure, hydrogen was assumed to be trapped in the grain

boundaries which was consistent with the brittle intergranular fracture mode. Finally, results also showed that only the hydrogen trapped at the grain boundaries controlled the mechanical properties of the alloy. The hydrogen trapped at the interface between the hardening precipitates and the matrix or/and in the elastic stress field surrounding those precipitates in the 150/20 sample had no detrimental effect on the mechanical properties which made the grain boundaries the most critical microstructural parameter for HE in AA 7046. Further, with an “adequate” population of hardening precipitates in AA 7046, hydrogen

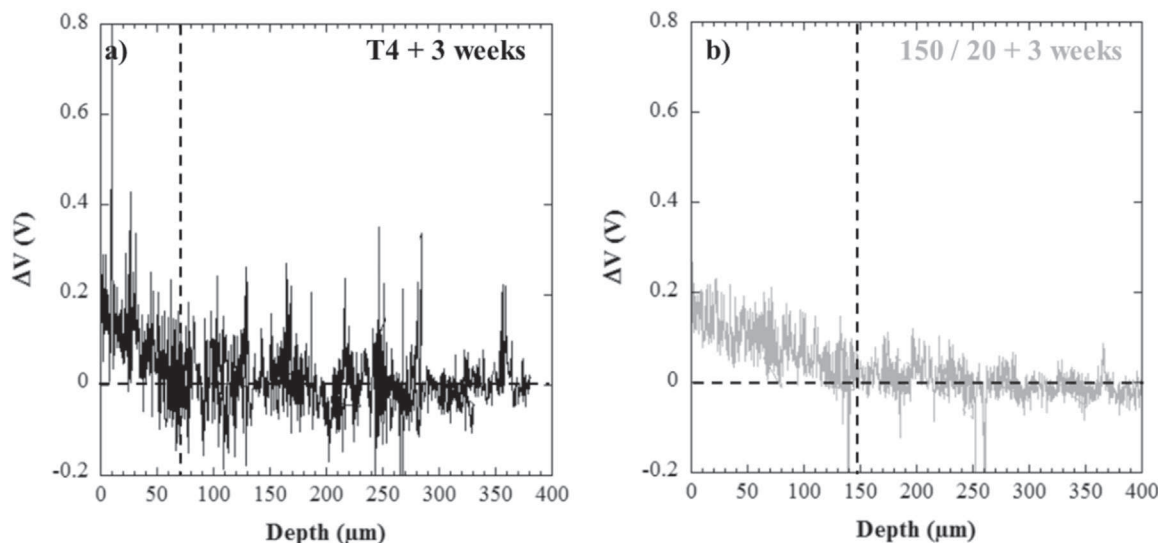


Fig. 9. SKPFM analyses of the depth still hydrogenated after 3 weeks of desorption at room temperature after cathodic charging for 72 h: a) T4 state, b) sample aged for 20 h at 150 °C (150/20).

could be trapped in these specific sites which allowed the grain boundaries to be less affected by hydrogen and then the susceptibility of AA 7046 to HE to be reduced.

4. Conclusions

The use of SKPFM associated with hydrogen cathodic charging method allowed the interactions between hydrogen and the microstructure of the AA 7046 to be investigated. The main conclusions were the following:

1. SKPFM measurements are relevant for the study of hydrogen diffusion and trapping in the Al-Zn-Mg alloys. Direct measurements did not allow the different populations of hydrogen to be distinguished but SKPFM measurements combined with desorption experiments allowed diffusible and trapped hydrogen to be clearly identified.
2. Global hydrogen amount measurements and SKPFM measurements highlighted the role of the hardening precipitates in hydrogen trapping and diffusion. Apparent diffusion coefficients, D_{app} , varying from $2 \cdot 10^{-10} \text{ cm}^2 \text{ s}^{-1}$ for the T4 metallurgical state to $6 \cdot 10^{-11} \text{ cm}^2 \text{ s}^{-1}$ for the samples aged at 150 °C for 48 h were measured showing clearly that the hardening precipitates were effective hydrogen trapping sites and led to a decrease of the hydrogen diffusion rate. Further, comparison of the results obtained for aged samples with different durations of ageing showed that the nature of the precipitates, presumably related to the coherence level of the matrix/precipitate interface, was a parameter of major importance in hydrogen trapping.
3. Finally, mechanical tests performed for hydrogen-charged samples allowed the role of the different populations of hydrogen in the loss of mechanical properties of AA 7046 to be explained. Hydrogen trapping at the grain boundaries led to a decrease of the mechanical properties of AA 7046 with brittle intergranular fracture mode. On the contrary, when hydrogen was trapped near the hardening precipitates, the grain boundaries were less affected by hydrogen leading to a higher resistance of the aged 7xxx alloys to HE.

Acknowledgements

The authors thank Professor Eric Andrieu for fruitful discussions. They also thank Marie-Christine Lafont and Alessandro Pugliara for the TEM observations. They also gratefully acknowledge Constellium Technology Center for its financial support and for providing the

materials.

References

- [1] L. Marretta, R. Di Lorenzo, F. Micari, J. Arinez, D. Dornfeld, Material substitution for automotive applications: a comparative life cycle analysis, in: *Leveraging Technology a Sustaining World Proceedings of the 19th CIRP Conference on Life Cycle Engineering*, University of California at Berkeley, Berkeley, USA, May 23–25, 2012, pp. 61–66. <http://doi.org/10.1007/978-3-642-29069-5_11>.
- [2] J. Hirsch, Recent development in aluminium for automotive applications, *Trans. Nonferrous Met. Soc. China* 24 (2014) 1995–2002, <[http://dx.doi.org/10.1016/S1003-6326\(14\)63305-7](http://dx.doi.org/10.1016/S1003-6326(14)63305-7)>.
- [3] M. Reboul, T. Magnin, T. Warner, Stress corrosion cracking of high strength aluminium alloys, in: ICAA, 1992.
- [4] K.R. Hebert, Trapping of hydrogen absorbed in aluminum during corrosion, *Electrochim. Acta* 168 (2015) 199–205, <<http://dx.doi.org/10.1016/j.electacta.2015.03.198>>.
- [5] W. Gruhl, *Zeitschrift fuer Metallkunde, Z. Fuer Met.* 75 (1984) 819–826.
- [6] G.M. Scamans, R. Alani, P.R. Swann, Pre-exposure embrittlement and stress corrosion failure in AlZnMg Alloys, *Corros. Sci.* 16 (1976), <[http://dx.doi.org/10.1016/0010-938X\(76\)90065-2](http://dx.doi.org/10.1016/0010-938X(76)90065-2)>.
- [7] L. Christodoulou, H. Flower, Hydrogen embrittlement and trapping in Al6%-Zn-3%-Mg, *Acta Metall.* 28 (1980) 481–487, <[http://dx.doi.org/10.1016/0001-6160\(80\)90138-8](http://dx.doi.org/10.1016/0001-6160(80)90138-8)>.
- [8] D. Najjar, Compétition entre les mécanismes de dissolution anodique et de fragilisation par l'hydrogène dans le processus de fissuration par corrosion sous contrainte de l'alliage Al-Zn-Mg-Cu 7150 sollicité en traction lente en milieu chloruré (NaCl 3%), 1994.
- [9] A.S. El-Amoush, An investigation of hydrogen-induced hardening in 7075-T6 aluminium alloy, *J. Alloy. Compd.* 465 (2008) 497–501, <<http://dx.doi.org/10.1016/j.jallcom.2007.10.126>>.
- [10] J.K. Park, A.J. Ardell, Precipitation at grain boundaries in the commercial alloy Al 7075, *Acta Metall.* 34 (1986) 2399–2409, <[http://dx.doi.org/10.1016/0001-6160\(86\)90143-4](http://dx.doi.org/10.1016/0001-6160(86)90143-4)>.
- [11] N.Ben. Ali, Caractérisation et modélisation micromécanique de la propagation de fissures fragiles par effet de l'hydrogène dans les alliages AA7xxx, 2011.
- [12] M.O. Speidel, *Hydrogen embrittlement*, in: A.R. Troiano, R. Gibala, R.F. Hehemann (Eds.), *Hydrogen Embrittlement, and Stress Corrosion Cracking*, 1984, pp. 271–296.
- [13] G.A. Young, J.R. Scully, The diffusion and trapping of hydrogen in high purity aluminum, *Acta Metall.* 18 (1998) 6337–6349, <[http://dx.doi.org/10.1016/0001-6160\(70\)90078-7](http://dx.doi.org/10.1016/0001-6160(70)90078-7)>.
- [14] H.K. Birnbaum, C. Buckley, F. Zeides, E. Sirois, P. Rozenak, S. Spooner, J.S. Lin, Hydrogen in aluminum, *J. Alloy. Compd.* 253–254 (1997) 260–264, <[http://dx.doi.org/10.1016/S0925-8388\(96\)02968-4](http://dx.doi.org/10.1016/S0925-8388(96)02968-4)>.
- [15] C. Larignon, J. Alexis, E. Andrieu, L. Lacroix, G. Odemer, C. Blanc, Investigation of Kelvin probe force microscopy efficiency for the detection of hydrogen ingress by cathodic charging in an aluminium alloy, *Scr. Mater.* 68 (2013) 479–482, <<http://dx.doi.org/10.1016/j.scriptamat.2012.11.026>>.
- [16] S. Evers, C. Senöz, M. Rohwerder, Spatially resolved high sensitive measurement of hydrogen permeation by scanning Kelvin probe microscopy, *Electrochim. Acta* 110 (2013) 534–538, <<http://dx.doi.org/10.1016/j.electacta.2013.04.171>>.
- [17] M. Koyama, A. Bashir, M. Rohwerder, S.V. Merzlikin, E. Akiyama, K. Tsuzaki, D. Raabe, Spatially and kinetically resolved mapping of hydrogen in a twinning-induced plasticity steel by use of scanning Kelvin probe force microscopy, *J.*

- Electrochem. Soc. 162 (2015) C638–C647, <http://dx.doi.org/10.1149/2.0131512jes>.
- [18] C.E. Buckley, H.K. Birnbaum, Characterization of the charging techniques used to introduce hydrogen in aluminum, *J. Alloy. Compd.* 330–332 (2002) 649–653, [http://dx.doi.org/10.1016/S0925-8388\(01\)01496-7](http://dx.doi.org/10.1016/S0925-8388(01)01496-7).
- [19] M. Nonnenmacher, M.P. O'Boyle, H.K. Wickramasinghe, Kelvin probe force microscopy, *Appl. Phys. Lett.* 58 (1991) 2921–2923, <http://dx.doi.org/10.1063/1.105227>.
- [20] P. Rometsch, Y. Zhang, S. Knight, Heat treatment of 7xxx series aluminium alloys – some recent developments, *Trans. Nonferrous Met. Soc. China* 24 (2003) 2003–2017, [http://dx.doi.org/10.1016/S1003-6326\(14\)63306-9](http://dx.doi.org/10.1016/S1003-6326(14)63306-9).
- [21] D. Godard, P. Archambault, E. Aeby-Gautier, G. Lapasset, Precipitation sequences during quenching of the AA 7010 alloy, *Acta Mater.* 50 (2002) 2319–2329, [http://dx.doi.org/10.1016/S1359-6454\(02\)00063-0](http://dx.doi.org/10.1016/S1359-6454(02)00063-0).
- [22] J.Z. Liu, J.H. Chen, X.B. Yang, S. Ren, C.L. Wu, H.Y. Xu, J. Zou, Revisiting the precipitation sequence in Al-Zn-Mg-based alloys by high-resolution transmission electron microscopy, *Scr. Mater.* 63 (2010) 1061–1064, <http://dx.doi.org/10.1016/j.scriptamat.2010.08.001>.
- [23] A. Kverneland, V. Hansen, G. Thorkildsen, H.B. Larsen, P. Pattison, X.Z. Li, J. Gjønnnes, Transformations and structures in the Al-Zn-Mg alloy system: a diffractometry study using synchrotron radiation and electron precession, *Mater. Sci. Eng. A* 528 (2011) 880–887, <http://dx.doi.org/10.1016/j.msea.2010.10.001>.
- [24] L.K. Berg, J. Gjønnnes, V. Hansen, X.Z. Li, M. Knutson-Wedel, G. Waterloo, D. Schryvers, L.R. Wallenberg, GP-zones in Al-Zn-Mg alloys and their role in artificial aging, *Acta Mater.* 49 (2001) 3443–3451, [http://dx.doi.org/10.1016/S1359-6454\(01\)00251-8](http://dx.doi.org/10.1016/S1359-6454(01)00251-8).
- [25] M. Dumont, W. Lefebvre, B. Doisneau-Cottignies, A. Deschamps, Characterisation of the composition and volume fraction of η' and η precipitates in an Al-Zn-Mg alloy by a combination of atom probe, small-angle X-ray scattering and transmission electron microscopy, *Acta Mater.* 53 (2005) 2881–2892, <http://dx.doi.org/10.1016/j.actamat.2005.03.004>.
- [26] X.Z. Li, V. Hansen, J. Gjønnnes, L.R. Wallenberg, HREM study and structure modeling of the η' phase, the hardening precipitates in commercial Al-Zn-Mg alloys, *Acta Mater.* 47 (1999) 2651–2659, [http://dx.doi.org/10.1016/S1359-6454\(99\)00138-X](http://dx.doi.org/10.1016/S1359-6454(99)00138-X).
- [27] B. Dubost, P. Sainfort, Durcissement par précipitation des alliages d'aluminium, *Tech. l'Ingénieur* (2015) 1–37.
- [28] P. Fernandez, G. Gonzalez, I. Alfonso, I.A. Figueroa, Hardness-lattice parameter correlation for aged Al-Zn-Mg alloys, *J. Mater. Sci. Technol.* 26 (2010) 1083–1088, [http://dx.doi.org/10.1016/S1005-0302\(11\)60005-4](http://dx.doi.org/10.1016/S1005-0302(11)60005-4).
- [29] Y. Iijima, S.I. Yoshida, H. Saitoh, H. Tanaka, K.I. Hirano, Hydrogen trapping and repelling in an Al-6 wt% Zn-2 wt% Mg alloy, *J. Mater. Sci.* 27 (1992) 5735–5738, <http://dx.doi.org/10.1007/BF01119730>.
- [30] J.R. Scully, G.A. Young Jr, S.W. Smith, Hydrogen solubility, diffusion and trapping in high purity aluminum and selected Al-base alloys, *Mater. Sci. Forum* 331–337 (2000) 1583–1600, <http://dx.doi.org/10.4028/www.scientific.net/MSF.331-337.1583>.
- [31] S. Frappart, Des éléments de compréhension sur les mécanismes de transport et de ségrégation de l'hydrogène dans les aciers martensitiques trempés et revenus à haute limite d'élasticité, Université de La Rochelle, 2014, <https://tel.archives-ouvertes.fr/tel-01016688/document>.
- [32] A. Fredholm, Monocristaux d'alliages base nickel : relation entre composition, microstructure et comportement en fluage à haute température, Ecole des Mines de Paris, 1987, <https://www.theses.fr/032497873>.
- [33] C. Wolverton, Crystal structure and stability of complex precipitate phases in Al-Cu-Mg-(Si) and Al-Zn-Mg alloys, *Acta Mater.* 49 (2001) 3129–3142, [http://dx.doi.org/10.1016/S1359-6454\(01\)00229-4](http://dx.doi.org/10.1016/S1359-6454(01)00229-4).
- [34] L. Hadjadj, R. Amira, D. Hamana, A. Mosbah, Characterization of precipitation and phase transformations in Al-Zn-Mg alloy by the differential dilatometry, *J. Alloy. Compd.* 462 (2008) 279–283, <http://dx.doi.org/10.1016/j.jallcom.2007.08.016>.
- [35] N. Takano, Hydrogen diffusion and embrittlement in 7075 aluminum alloy, *Mater. Sci. Eng. A*. 483–484 (2008) 336–339, <http://dx.doi.org/10.1016/j.msea.2006.08.144>.
- [36] D. Dumont, Relations microstructure/Ténacité microstructure/ténacité dans les alliages aéronautiques de la série 7000, *Inst. Natl. Polytech. Grenoble* (2001).
- [37] T. Malis, M.C. Chaturvedi, Grain-boundary segregation in an Al – 8 wt% Mg alloy, *J. Mater. Sci.* 17 (1982) 1479–1486.
- [38] E. Pouillier, A.F. Gourgues, D. Tanguy, E.P. Busso, A study of intergranular fracture in an aluminium alloy due to hydrogen embrittlement, *Int. J. Plast.* 34 (2012) 139–153, <http://dx.doi.org/10.1016/j.ijplas.2012.01.004>.
- [39] H. Kamoutsi, G.N. Haidemenopoulos, V. Bontozoglou, P.V. Petroyiannis, S.G. Pantelakis, Effect of prior deformation and heat treatment on the corrosion-induced hydrogen trapping in aluminium alloy 2024, *Corros. Sci.* 80 (2014) 139–142, <http://dx.doi.org/10.1016/j.corsci.2013.11.021>.